Chinese Chemical Letters 34 (2023) 107951

Contents lists available at ScienceDirect

Chinese Chemical Letters

journal homepage: www.elsevier.com/locate/cclet

Degradable nanocatalyst enables antitumor/antibacterial therapy and promotion of wound healing for diabetes *via* self-enhanced cascading reaction

Xiang Wang[a,1], Cheng Ding[b,1], Ziwen Zhang[a,1], Chunlin Li[c], Dongmiao Cao[a], Linjing Zhao[a], Guoying Deng[c], Yu Luo[a], Chunping Yuan[a], Jie Lu[a], Xijian Liu[a,*]

[a] *School of Chemistry and Chemical Engineering, Shanghai Engineering Technology Research Center for Pharmaceutical Intelligent Equipment, Shanghai Frontiers Science Research Center for Druggability of Cardiovascular Noncoding RNA, Institute for Frontier Medical Technology, Shanghai University of Engineering Science, Shanghai 201620, China*

[b] *Affiliated Sixth People's Hospital, Shanghai JiaoTong University, Shanghai 200233, China*

[c] *Trauma Center, Shanghai General Hospital, Shanghai Jiaotong University School of Medicine, Shanghai 201620, China*

ARTICLE INFO

Article history:
Received 22 July 2022
Revised 17 October 2022
Accepted 23 October 2022
Available online 26 October 2022

Keywords:
Self-cascade reaction
Starvation therapy
Chemodynamic therapy
Antitumor
Antibacterial
Wound healing

ABSTRACT

Diabetic patients often have problems such as residual tumor and wound infection after tumor resection, causing severe clinical problems. It is urgent to develop effective therapies to reach oncotherapy/anti-infection/promotion of wound healing combined treatment. Herein, we propose CS/MnO_2-GOx (CMGOx) nanocatalysts for the specific catalytic generation of $^{\bullet}OH$ to inhibit tumors and bacteria in a hyperglycemic environment. The good biocompatible chitosan (CS), as a carrier for the catalyst, exhibits excellent antibacterial effect as well as promotes wound healing. Glucose oxidase (GOx) is loaded on the surface of CS nanoparticles to generate H_2O_2 and gluconic acid by consuming glucose (starvation therapy, ST) and O_2. The MnO_2 depletes glutathione (GSH) to produce Mn^{2+}, amplifying oxidative stress and further promoting the activity of Mn^{2+}-mediated Fenton-like reaction to produce $^{\bullet}OH$ (chemodynamic therapy, CDT) in weak acidic environment. Moreover, the produced gluconic acid lowers the pH of the environment, enhancing chemodynamic therapy (ECDT). The tumor cells and bacteria are efficiently eliminated by the synergistic effect of ST and ECDT. The MnO_2 nanoparticles at neutral environment decomposes H_2O_2 into O_2, which cooperate with CS to promote healing. The self-enhanced cascade reaction of CMGOx *in situ* exhibits excellent effects of antitumor/antibacterial therapy and promotion of wound healing, offering a promising integrated treatment for diabetic patients after tumor surgical resection.

According to statistics, countless patients suffer from diabetes, a metabolic disease characterized by hyperglycemia [1,2]. Epidemiological researches exhibit that diabetic possess a higher risk of suffering cancer [3]. Surgical excision is one of the primary methods to treat and inhibit tumor progression [4,5]. For example, skin cancer is a frequent malignant tumor whose primary treatment is surgery in clinical [6,7]. However, much of the normal skin tissue surrounding the tumor cells have to be removed for preventing recurrence, leading to large skin defects, subsequent infection, and chronic wound healing [8–10]. Even with enhanced surgical resection techniques, some residual tumor micro infiltration still predisposes to tumor recurrence. At the same time, diabetes patients are more likely to develop bacterial infections in a wound which are not easy to recover. High blood glucose provides better microenvironment for bacteria to grow [11]. It becomes a significant challenge to achieve tumor treatment and anti-infection after surgical resection of tumors.

Enzymes as traditional, highly specific antitumor and antibacterial agents are well established in antitumor and antibacterial research [12,13]. The particular enzymes catalyze substrate oxidation to generate hydrogen peroxide (H_2O_2), which can degrade bacterial membranes and disturb tumor cell propagation [12]. Glucose oxidase (GOx) is an oxygen-demanding dehydrogenase, which has been developed for glucose consumption in tumor starvation therapy (ST) [14,15]. GOx can specifically catalyze glucose to generate gluconic acid and H_2O_2 [16,17]. The produced H_2O_2 can be used for antitumor/antibacterial therapy in diabetic patients [18,19]. With the advantage of generating H_2O_2 by consuming

* Corresponding author.
E-mail address: liuxijian@sues.edu.cn (X. Liu).
[1] These authors contributed equally to this work.

https://doi.org/10.1016/j.cclet.2022.107951
1001-8417/

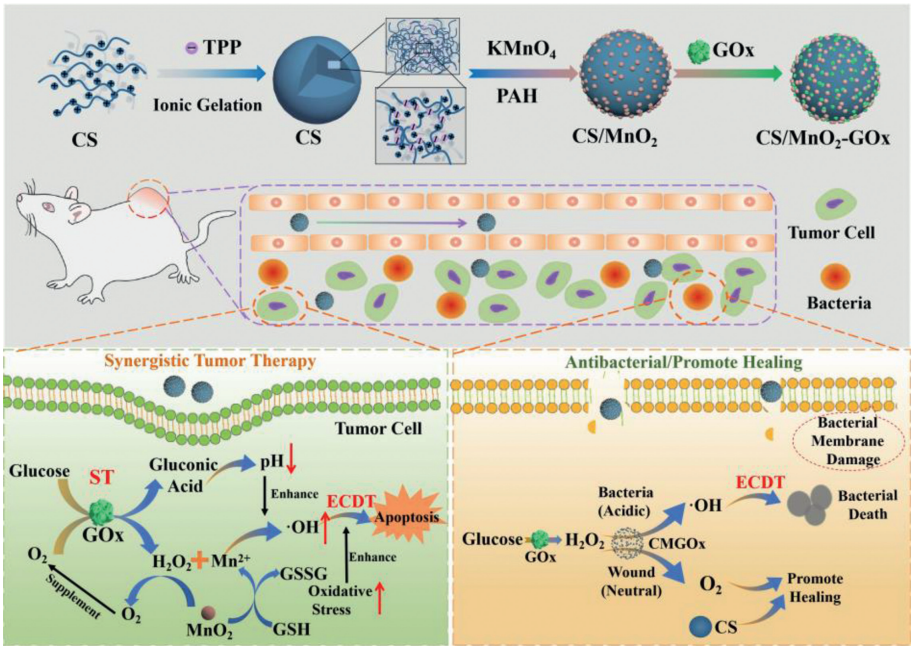

Scheme 1. Schematic illustrations of the process for synthesizing the CMGOx catalyst, and antitumor and antibacterial mechanism through self-enhanced cascade catalysis.

glucose needed for cancer cells and bacterial growth, GOx has been widely applied as an antibacterial agent in food processing and anticancer agent for tumor therapy [20–22]. However, the oxidative capacity of H_2O_2 is too weak to reach satisfied anticancer and antibacterial effects. The H_2O_2 can be catalyzed into more potent ·OH (one of the ROS) by prepared nano-enzyme [23–26]. ROS can promote immune cells to express pro-inflammatory cytokines, resulting in inflammatory response and clearance of pathogens [27–30]. Thus, the combination of GOx and nano-enzyme can treat tumors and wounds infection by generating H_2O_2 and then catalyzing it into ·OH *in situ*, reaching a better therapeutic effect. Shao *et al.* designed a bio-nanoreactor based on GOx for tumor cell membrane camouflage. This biomimetic nanoreactor could inhibit tumor cells by consuming glucose through GOx to cut off nutrients [31,32]. Li *et al.* investigated a nanozyme (GFeF), which can generate ·OH through the self-cascade reaction between GOx and metal ions to treat diabetic wound infection [33]. However, the application of GOx-based nanocomposites for promotion of wound healing in diabetic patients after tumor surgery has not been well reported. Probably, it is still a great challenge to reach antitumor/antibacterial therapy and promotion of wound healing in a hyperglycemic environment for the enzyme-based nanocomposites. Therefore, it is essential to design nanomaterials to achieve excellent wound healing after tumor surgery for diabetic patients.

Hence, we proposed an antitumor, antibacterial and healing promotion agent for diabetic tumor patients based on high biocompatible CS nanoparticles (Scheme 1). The MnO_2 grew on the CS surface through redox reactions, and then GOx loaded on the surface, forming CS/MnO_2-GOx (CMGOx). The GOx consumed the glucose (starvation therapy, ST) to generate H_2O_2 and decreased the glucose concentration in the local microenvironment to promote antibacterial and anti-tumor effects. In the faintly acid tumor and infection microenvironment, MnO_2 depleted glutathione (GSH) to produce Mn^{2+}, amplifying oxidative stress. Simultaneously, GOx catalyzed the production of gluconic acid though consuming glucose and efficiently promoted the activity of Mn^{2+}-mediated Fenton-like reaction to produce ·OH, enhancing chemodynamic therapy (ECDT). The produced ·OH efficiently induced the death of tumor cells and bacteria, meanwhile the cooperation between CS and MnO_2 could prevent infection and promote tissue regeneration. This CMGOx utilized endogenous substances to carry out self-enhanced cascade catalytic reactions, demonstrating excellent therapeutic effect. Thus, the CMGOx provided a comprehensive solution for diabetic patients to reach antitumor/antibacterial therapy and promotion of wound healing *via* ECDT and ST.

We firstly synthesized CS nanoparticles as base for CMGOx nanocomposites. The TEM images of Figs. S1a and b (Supporting information) showed that the obtained CS had a spherical structure. After growing MnO_2 on the CS surface, the surface of nanoparticles was rough and the particle size became larger (Figs. S1c and d in Supporting information). The slight agglomeration of CM in TEM images may be due to chitosan tending to agglomerate after solvent evaporation. The element mapping confirmed the uniform distribution of C, N, O and Mn in the CS@MnO_2 (CM) nanocatalyst (Fig. S1e in Supporting information), indicating that MnO_2 was uniformly grown on the surface. It can be seen from DLS that the composites are well dispersed in aqueous solution (Fig. S1f in Supporting information). The hydrated size of the CM nanocatalyst was about 182 nm. From the X-ray diffraction (XRD) patterns of CS and CM in Fig. S1g (Supporting information), CM exhibited similar peaks of CS and also exhibited characteristic peaks of MnO_2 (JCPDS No. 44-0992)). The lattice spacing is 0.258 nm, which matched the (311) plane of MnO_2 (Fig. S2a in Supporting information). The characteristic absorption spectrum of CM was well agreement with that of MnO_2 (Fig. S2b in Supporting information), which indicated the successful introduction of MnO_2. There was a significant enhancement of the absorption peak of CMGOx around 390 nm, confirming the successful encapsulation of GOx. The ζ-potential changes of materials at the synthesis stage were monitored (Fig. S1h in Supporting information). The positive charge of CS (+12.1 mV) was increased to +23 mV after introducing MnO_2, then ζ-potential decreased to 10 mV after loaded GOx, indicating the adsorption of GOx onto CM. From the FT-IR spectra of CS and CM (Fig. S2c in Supporting information), CS could be observed an O-H bond at 3421 cm^{-1} accompanied by an amide stretching vibration of -NHCO- at 1659 cm^{-1}. Moreover, the CH_3, -C-O and -C-N vibrations were exhibited at 1382 cm^{-1}, 1155 cm^{-1} and 1084 cm^{-1}, respectively. The vibrations of the

Mn-O bond of the MnO_2 particles were associated with a peak at 540 cm^{-1} [34,35]. In summary, the results confirmed the successful preparation of CMGOx.

The catalytic mechanism based on CMGOx is a series of cascade reactions. The glucose is oxidized into gluconic acid and H_2O_2 through catalyzing by GOx, and then MnO_2 catalyzes H_2O_2 to •OH under acidic conditions. The detection of free radicals is achieved by 3,3′,5,5′-tetramethyl-benzidine (TMB). The generated ROS (•OH) oxidized colorless TMB to blue TMB cationic radical (oxTMB), which exhibited absorption peak at 652 nm [28]. Firstly, we monitored the catalytic activity of MnO_2 through TMB. As shown in Fig. S3a (Supporting information), the coexistence of CM and H_2O_2 oxidized TMB to blue oxTMB and the characteristic peak of 652 nm appeared, confirming the catalytic activity of MnO_2. In contrast, the control group had no change in color and absorbance. In general, a fatal disadvantage of these nano-catalysts is that their optimal catalytic activity is usually at pH 3–4, which severely limits their application in reactions [36]. The GOx can catalyze naturally nontoxic and biocompatible glucose into gluconic acid and H_2O_2. The production of gluconic acid can significantly lower the pH of the environment and enhance the cascade reaction. First of all, we measured glucose concentration and pH changes in solution to assess the catalytic activity of GOx. When glucose was catalyzed by GOx, pH value of the system decreased from 6.5 to 3.0. The pH gradually decreased as the reactant-glucose content increased, demonstrating the production of more gluconic acid (Fig. S4 in Supporting information). Methyl red solution is yellow when pH value above 6.2 and is red below 4.4, respectively [37]. As shown in Figs. S3b and c (Supporting information), the indicator appeared yellow (pH values greater than 6.2) in the control group, while methyl red changed from yellow to red when CMGOx was mixed with glucose, indicating that the pH of the system decreased from 6.5 to below 4.4. The above results manifested that the reaction of GOx with glucose successfully generated a large amount of gluconic acid and reduced pH value of the environment. We also confirmed the activity of CMGOx at different pH value. The pH value of solution had a slight decrease to 7.2 at initial pH 7.4 in the presence of glucose and CMGOx (Figs. S3e and f in Supporting information). On the contrary, CMGOx showed a stronger activity to catalyze glucose at initial pH 6.5, and the pH value of solution decreased to 2.9, which was very suitable for Fenton reaction [36]. The indicator changed from yellow to red, confirming that GOx has a better catalytic performance in the slightly acidic situation. Thus, a slightly acidic environment with a high glucose concentration will lead to a better catalytic performance.

The above results lay a solid foundation for subsequent *in vivo* application. It is well known that the bacterial and tumor environments are weakly acidic. Based on the above experiments, CMGOx can reduce the environmental pH and generate more •OH in the environments of bacterial infection and tumor [38].

As mentioned previously, the peroxidase activity of CM NCs and the catalytic nature of GOx for glucose have been demonstrated, we further investigated the cascade catalytic reaction by CMGOx. The solution of CMGOx, glucose and TMB after co-incubation showed a strong characteristic peak of oxTMB (Fig. 1a). In contrast, the peak was not observed in the other groups. Only the solution color in group 6 (CMGOx + glucose) showed a blue color, which also proved that the cascade reaction could only occur in the presence of glucose and CMGOx together. To further demonstrate that gluconic acid can enhance the catalytic process, we monitored the absorbance change of the supernatant solution after incubation of glucose, CMGOx and TMB at different times. The oxTMB absorbance of the solution increased faster with time, confirming that the generated gluconic acid enhanced the catalytic activity of CMGOx (Fig. 1b). Based on TMB colorimetric analysis, it has been demonstrated that CMGOx nanocatalysts can achieve self-enhanced enzymatic cascade reaction. In detail, when the CMGOx nanocatalysts, glucose and TMB co-existed, the solution gradually turned blue and a significant absorption peak appeared at 652 nm, proving that the cascade reaction occurred and produced a large amount of •OH by CMGOx. The gluconic acid can be produced by loaded GOx, which provides a compatible catalytic environment to efficiently produce H_2O_2 and then greatly enhances CMGOx activity to generate more toxic •OH due to acid condition favoring the Fenton reaction.

Decreased absorbance of methylene blue (MB) at 660 nm demonstrated the generation of free radicals [39–41]. In Fig. 1c and Fig. S5 (Supporting information), the absorbance of MB had only a little decline in glucose + pH 7.4 group. While the absorbance of MB decreased significantly in glucose + pH 6.5 group, whose drop-out value of 60 min was four times more than that of glucose + pH 7.4 group. The decrease in absorbance of MB demonstrated the successful generation of ROS from the self-cascade reaction in the presence of glucose. A slightly acidic environment with glucose significantly enhanced catalytic performance of CMGOx and accelerated cascade reaction of CMGOx due to acid condition favoring Fenton reaction.

O_2 production and GSH depletion can likewise be used as an adjunct strategy for amplifying oxidative stress to improve therapeutic efficacy [42,43]. As shown in Fig. 1d, a large amount of O_2 was generated in the CMGOx + H_2O_2 system at neutral pH. The O_2 generation in the CMGOx group increased exponentially, and the control group had almost no O_2 generation. According to the previous studies, the generation of O_2 comes from the decomposition of H_2O_2 catalyzed by MnO_2 [44,45], which can promote wound healing. Thus, the GSH depletion was measured by Ellman's method. The UV absorbance of GSH decreased significantly after incubation with CM and CMGOx, demonstrating that GSH was oxidized (Fig. 1e). In comparison, no significant change was observed after CS treatment. The UV absorption progressively decreased with the increase of CMGOx NCs concentration (Fig. 1f), indicating the effective deprivation ability of nano-catalysts toward GSH. These phenomena suggest that CMGOx could deplete GSH to generate Mn^{2+} ions, enhancing CDT (Fig. 1g) [46,47]. The reaction process of GSH depletion is as follows (Eq. 1):

$$MnO_2 + GSH \rightarrow Mn^{2+} + GSSG \quad (1)$$

The biodegradation behavior of CMGOx was assessed by accumulated release of Mn at pH 7.4 (healthy body fluids) and pH 6.5 (tumor or bacterial environment) (Fig. S6a in Supporting information). During the degradation period of 48 h, the release rate of Mn from CMGOx in an acidic medium was higher than that in a neutral medium. It means that CMGOx is easily degraded in acidic environment and releases more Mn ions for acquiring a better catalytic effect. We also observed the degradation of CMGOx by TEM. In acidic PBS, the morphologies of CMGOx remained spherical at 24 h, but the particle size decreased significantly and porous shape appeared (Fig. S6b in Supporting information). As the time was extended to 48 h, CMGOx exhibited significant structural collapsed and degraded to ultra-small nanoparticles, which were easily metabolized out of the body (Fig. S6c in Supporting information).

The bio-elimination behavior of CMGOx NCs *in vivo* was further studied. CMGOx (20 mg/kg) was injected intravenously into mice. Most of the Mn was retained in the spleen after 2 h, then gradually decreased at subsequent time points (Fig. S6d in Supporting information). After 48 h, Mn content was very low in all organs, indicating that CMGOx can be effectively cleared from mice. Notably, high levels of Mn could be detected in the feces at 12 h after injection of CMGOx solution (Fig. S6e in Supporting information). The decrease in Mn levels over time represented the gradual elimination of CMGOx. After 7 days, CMGOx almost completely metabolized out of the body. After intravenous injection, CMGOx showed a circulat-

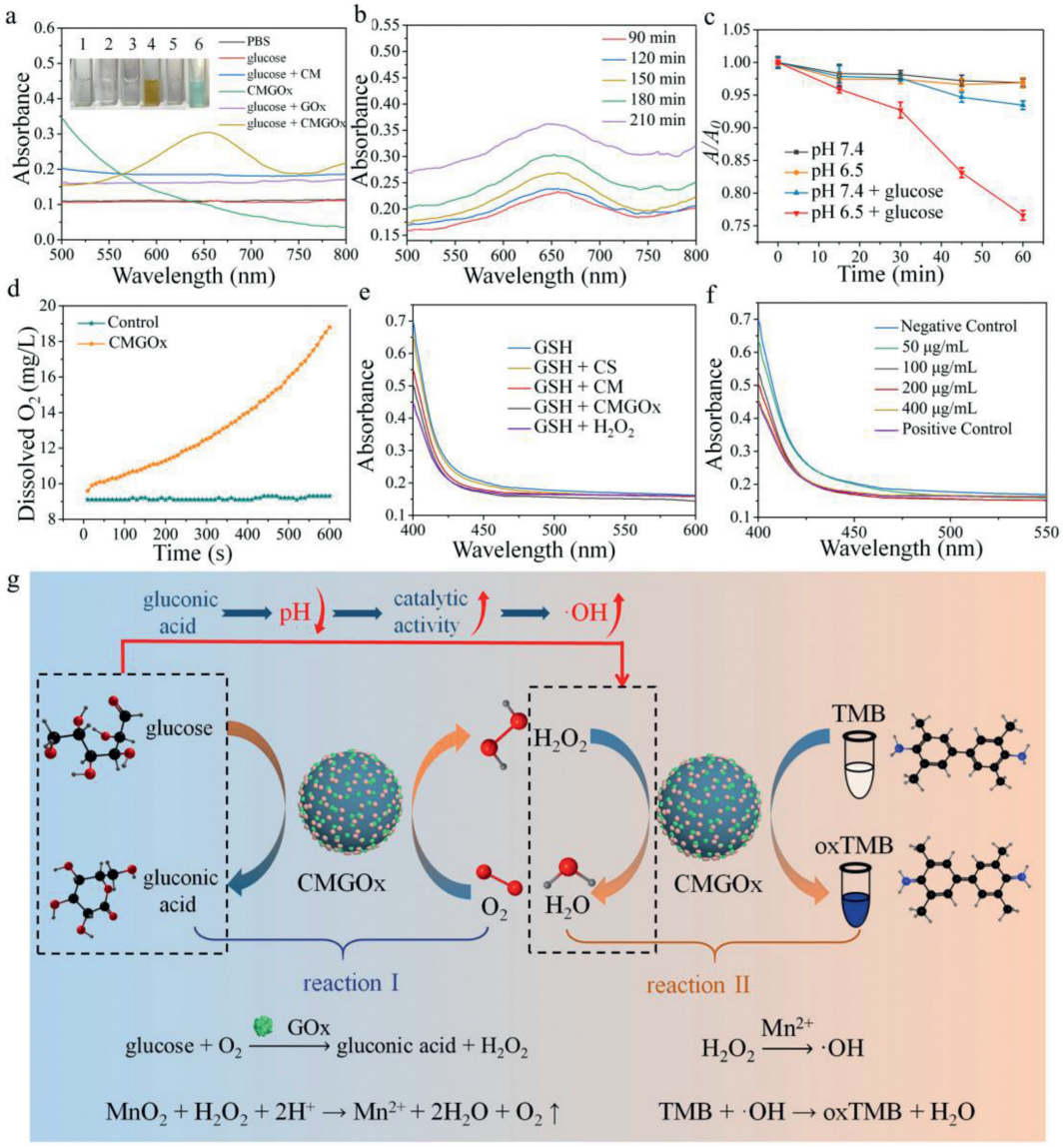

Fig. 1. (a) UV–vis spectra of various reaction solutions containing TMB. Inset: color of different reaction mixture. (b) UV–vis absorption spectra of PBS solution containing CMGOx, glucose and TMB. (c) The absorbance of MB containing CMGOx at pH 6.5/pH 7.4 with or without the addition of glucose. (d) O_2 production in the glucose solution containing CMGOx. Corresponding GSH depletion in (e) different groups and (f) different concentrations of CMGOx. (g) Schematic illustrations of glucose oxidation and ·OH generation catalyzed by CMGOx nanocomposite.

ing half-life of 2.29 h in the bloodstream (Fig. S6f in Supporting information). From these results, it suggested that CMGOx gradually degraded into small nanoparticles or ions to speed up their elimination from the reticuloendothelial system (RES) [48–51].

The antibacterial behavior of CMGOx was further investigated by direct observation of bacterial destruction and morphological changes using scanning electron microscopy (SEM) (Fig. S7a in Supporting information). The number of *S. aureus* and *E. coli* decreased with time after treatment with CMGOx and glucose. Similarly, different groups were set up for more detailed discussion (Figs. S7b and c in Supporting information). Both bacteria incubated with PBS (group 1) and glucose (group 2) showed excessive bacterial survival. Groups 3 (glucose + CS) and 4 (glucose + CM) appeared weak antibacterial effect because of the antibacterial properties of CS itself. Group 5 (glucose + GOx) showed bacterial survival rates higher than 60% and 55% for *S. aureus* and *E. coli*, respectively. The antibacterial effect of GOx mainly comes from the production of H_2O_2, but it cannot efficiently kill bacteria. In contrast, group 6 (glucose + CMGOx) led to a significant decrease in bacterial survival, since H_2O_2 was produced and then MnO_2 efficiently catalyzed H_2O_2 into toxic ·OH to kill bacteria. Thus, the maximum antibacterial effect was achieved by synergistic effect of ·OH and CS. All above results match the conclusion of plate counting method (Figs. S7b and c). As shown in Figs. S7d and S8 (Supporting information), untreated *S. aureus* cells exhibited smooth spherical surfaces (Fig. S7d(1)). After incubation with different materials (Fig. S7d(2–4)), the bacterial surface was rough and slightly damaged, mainly due to the antibacterial effect of CS. The surface of bacteria in group 5 was fractionally wrinkled due to the production of H_2O_2 (Fig. S7d). Apparently, all bacteria membranes treated with glucose + CMGOx collapsed due to the production of toxic ·OH and the excellent antibacterial ability of CS (group 5, Fig. S7d). For *E. coli*, the morphological changes were consistent with *S. aureus* (Figs. S7e and S9 in Supporting information). Furthermore, when the bacteria and methyl red were co-existed with glucose + CMGOx (insets in Figs. S7d and e), a reddish color was

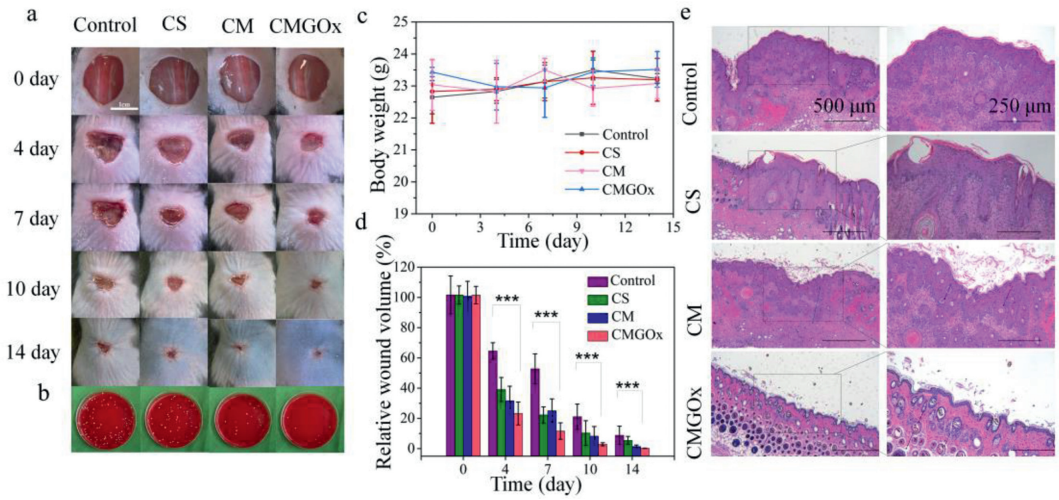

Fig. 2. (a) Wound photograph of diabetic mice. (b) Photograph of bacterial colonies in wound tissue of mice. (c) Body weights and (d) relative wound volumes of mice at different time ($^{*}P < 0.05$, $^{**}P < 0.01$ and $^{***}P < 0.001$, $n = 3$). (e) H&E staining images of the traumatic tissue after different treatments.

observed, indicating the production of gluconic acid. Overall, the generated gluconic acid enhanced the self-cascade reaction to produce ROS which exerted a synergetic antibacterial effect with CS.

ROS can oxidize the intracellularly labeled DCFH to produce the fluorescent substance, DCF, so its fluorescence value represents the relative amount of ROS. The CMGOx treatment of *S. aureus* resulted in the production of large amounts of ROS, laying the foundation for later *in vivo* antibacterial application (Fig. S10 in Supporting information).

Firstly, the cytotoxicity of CMGOx nanoparticles on melanoma A375 cells and normal HUVE cells was examined by the standard cell counting kit (CCK-8) method. CMGOx had no adverse effect on the proliferation of normal cells, even at high concentration as 400 μg/mL (Fig. S11a in Supporting information). Furthermore, it was found that cell survival decreased in a dose-dependent manner when incubated with CMGOx at pH 6.5. CMGOx (200 μg/mL) inhibited more than 75% A375 tumor cells (Fig. S11b in Supporting information). These results suggest that a slightly acidic environment is more conducive to the cascade catalytic reaction of CMGOx, which triggers massive production of $^{\bullet}OH$ to kill tumor cells.

To evaluate the antibacterial performance of the self-cascade agent CMGOx *in vivo*, we constructed a bacterial infection model in diabetic mice. Mice were divided into control group (group I), CS (group II), CM (group III) and CMGOx (group IV), with three mice in each group. The CMGOx group had better healing effect than the other three groups. The wounds of mice treated by CMGOx group gradually formed a scar on day 3, and the scar gradually disappeared (Fig. 2a). To better assess the antibacterial effect, plate counts were used to quantifying bacteria in wound of different groups on day 14 (Fig. 2b). Nearly all bacteria in the CMGOx group disappeared, exhibiting the most effective sterilization effect. No mice manifested any significant change in body weight during the treatment period (Fig. 2c). Quantitative evaluation of wound healing in the defect area showed substantial differences in early healing rates. After 7 days of treatment, the healing ration of CMGOx (88.4%) was higher than control group (47.3%), CS group (77.7%) and CM group (74%) (Fig. 2d). H&E staining of wound tissue was used to assess the wound healing (Fig. 2e). A small amount of newly formed epidermis was visible around the wound surface in the CS groups. The CMGOx group had fewer inflammatory cells, thickest dermal tissue, most abundant skin appendages (*e.g.*, hair follicles), and the most complete tissue remodeling than other groups. H&E staining of major organs validated the high safety profile of CMGOx (Fig. S12 in Supporting information). Firstly, CMGOx undergone a series of reactions to produce ROS for killing bacterial. GOx is easily degraded when exposed to biological conditions [52]. Then, coupled with the neutral conditions of the wound, the H_2O_2 in the later stage was greatly decomposed, which was beneficial to the later wound repair, and the presence of CS also enhanced the repair effect [53–56].

The anti-tumor effect of CMGOx was further confirmed in A375 tumor-bearing mice. Physiological saline (control group) and nanomaterials of different groups were administered intravenously to study the therapeutic effect. In the tumor suppression assessment, CMGOx showed a best suppressive effect (Figs. 3a and b). The highly toxic $^{\bullet}OH$ generated by CMGOx NCs through sequential bio/chemically catalytic reactions acquired satisfactory tumor suppression. In this process, CMGOx NCs efficiently consumed glucose nutrients to generate lots of H_2O_2, which was catalyzed into $^{\bullet}OH$ by MnO_2 NPs in the tumor acid environment. The resulting toxic $^{\bullet}OH$ could kill cancer cells through the mitochondria-mediated apoptosis pathway [8,57,58]. During 14 days of treatment, mice in all treated groups showed no noticeable changes in body weight (Fig. 3c), indicating treatment by CMGOx NCs did not cause perceptible toxicity. Tumors of mice were dissected, which provided visual evidence that CMGOx could effectively inhibit tumor growth. H&E staining of tumors further demonstrated the superior capabilities of CMGOx to cause tumor apoptosis (Fig. 3d). Moreover, H&E staining of major organs was executed after injection of 14 days to assess the safety of materials *in vivo* (Fig. 3e). Pathological photographs of CMGOx group showed negligible damage to organs after treatment.

Even with enhanced surgical resection techniques, some residual tumor micro infiltration still predisposes to tumor recurrence. Meanwhile, tumor resection always leads to deficiency of some normal tissues. Therefore, it is vital to create biomaterials that are able to prevent tumor recurrence and promote healing during postoperative treatment. To assess the postoperative tumor treatment and wound recovery efficacy of CMGOx, we used a resection model with A375 tumor-bearing mice. As shown in Fig. S13a (Supporting information), some parts of tumors in mice were excised by conventional surgery. Subsequently, saline (control) and CMGOx NCs were injected into the tumor site. Notably, the remaining tumors of mice in the CMGOx group disappeared, and the wound healing was rapid, and there was no perceptible difference between normal skin and wound skin (Figs. S13b and c in Supporting

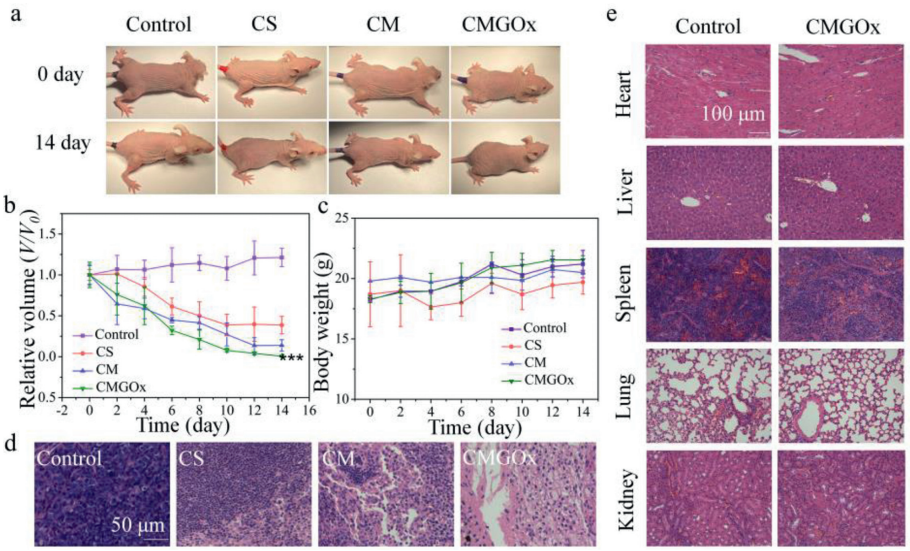

Fig. 3. (a) Photographs of mice after different treatments. Relative tumor volumes (b) and body weights (c) of mice in different groups ($^{*}P < 0.05$, $^{**}P < 0.01$ and $^{***}P < 0.001$, $n = 3$). (d) Staining of tumor tissue after 8 days of different treatment. (e) H&E Staining of main organs after 14 days of treatment.

information). However, the volume of tumor in the control group had some rise and the wound still existed after 14 days. None group had significant change in the bodyweight, further proving good safety of the treatment (Fig. S14 in Supporting information). CMGOx is sensitive to weakly acidic environment. The normal cell environment of the wound is neutral, and very little ·OH can be produced by CMGOx, so it has no appreciable toxic and side effects. These results demonstrated that self-cascade-generated ROS by CMGOx could effectively inhibit tumors and prevent bacterial infection. Secondly, the consumption of glucose could further use ST to eliminate tumors, and achieve the combined treatment effect of CDT and ST. Difficulty of wounds healing is mainly due to high glucose and bacterial infection at the wound. The presence of CMGOx can deplete glucose in the environment while killing bacteria in the wound. After the elimination of bacteria and tumors, the wound environment is neutral, and GOx is gradually degraded, producing less H_2O_2, which is beneficial to wound repair [54]. In particular, the introduction of CS could prevent wound infection and promote wound healing [55,56]. Therefore, the prepared CMGOx NCs have promising applications in preventing of tumor recurrence and promoting wound healing after surgical resection.

In conclusion, we developed degradable self-enhanced cascade catalysts-CMGOx for antitumor/antibacterial therapy and promotion of wound healing toward diabetes patients. The CMGOx not only generated H_2O_2, but also catalyzed it into ·OH through self-enhanced cascade reactions to inhibit tumors and bacteria in a hyperglycemic environment, simultaneously consuming GSH to enhance oxidative stress. The CMGOx also consumed glucose in tumors to starve tumor cells. In addition, CMGOx utilized CS as a carrier, which inhibited bacteria as well as promoted wound healing. The H_2O_2 in pH of neutral environment was greatly decomposed, which further improve healing. This work suggests that CMGOx has excellent effects on antitumor/antibacterial therapy and promotion of wound healing, offering a promising integrated treatment for diabetes after tumor resection.

Declaration of competing interest

The authors declare that they have no known competing financial interests or personal relationships that could have appeared to influence the work reported in this paper.

Acknowledgments

All animal procedures are according to the National Laboratory Animal Care and Use Regulations and are supported by the Laboratory Animal Welfare and Ethics Committee of the Clinical Center of Shanghai First People's Hospital (No. 2020AWS0065).

This work was financially supported by the National Natural Science Foundation of China (Nos. 21978165, 92156020), Science and Technology Commission of Shanghai (No. 20DZ2255900), and Class III Peak Discipline of Shanghai—Materials Science and Engineering (High-Energy Beam Intelligent Processing and Green Manufacturing).

Supplementary materials

Supplementary material associated with this article can be found, in the online version, at doi:10.1016/j.cclet.2022.107951.

References

[1] G. Guo, T. Gong, H. Shen, et al., Adv. Funct. Mater. 31 (2021) 2100795.
[2] C. Zhang, S. Hong, M.D. Liu, et al., J. Control. Release 320 (2020) 159–167.
[3] S.C. Chen, Y.C. Su, Y.T. Lu, et al., PLoS One 9 (2014) e109961.
[4] L. Zhou, Y. Xi, Y. Xue, et al., Adv. Funct. Mater. 29 (2019) 1806883.
[5] M.B. Ishak Gabra, Y. Yang, H. Li, et al., Nat. Commun. 11 (2020) 3326.
[6] Y. Xi, J. Ge, M. Wang, et al., ACS Nano 14 (2020) 2904–2916.
[7] E. Quintana, M. Shackleton, M.S. Sabel, et al., Nature 456 (2008) 593–598.
[8] Y. Su, X. Zhang, G. Ren, et al., Chem. Eng. J. 400 (2020) 125949.
[9] D. Li, T. Chen, Y. Zhang, Y. Xu, H. Niu, Adv. Healthc. Mater. 10 (2021) e2100716.
[10] Q. Yu, Y. Han, X. Wang, et al., ACS Nano 12 (2018) 2695–2707.
[11] Z. Xu, G. Liu, Q. Li, J. Wu, Nano Res. 15 (2022) 5305–5315.
[12] I. Lee, H.J. Cheon, M.D. Adhikari, et al., Int. J. Biol. Macromol. 155 (2020) 1520–1531.
[13] C. Wu, Y. Li, Z. Cheng, et al., Chin. Chem. Lett. 33 (2022) 4339–4344.
[14] Y. Yang, H. Wu, B. Liu, Z. Liu, Adv. Drug. Deliv. Rev. 179 (2021) 114004.
[15] X. Meng, Z. Lu, Q. Lv, et al., Acta Biomater. 145 (2022) 222–234.
[16] X. Qi, Q. Chen, Z. Chang, Y. Deng, Nano Res. 15 (2022) 5646–5652.
[17] M. Zhang, X. Liu, Q. Luo, et al., Chem. Eng. J. 389 (2020) 124450.
[18] L. Feng, R. Xie, C. Wang, et al., ACS Nano 12 (2018) 11000–11012.
[19] Z. Xu, G. Liu, J. Huang, J. Wu, ACS Appl. Mater. Interfaces 14 (2022) 7680–7689.
[20] Y. Ji, Z. Han, H. Ding, et al., ACS Appl. Mater. Interfaces 13 (2021) 17289–17299.
[21] N. Zhang, G. Shu, L. Shen, et al., Nano Res. 15 (2022) 5262–5272.
[22] X. Wang, X. Zhong, J. Li, Z. Liu, L. Cheng, Chem. Soc. Rev. 50 (2021) 8669–8742.
[23] J. Noh, B. Kwon, E. Han, et al., Nat. Commun. 6 (2015) 6907.
[24] X.L. Xu, N.N. Zhang, G.F. Shu, et al., ACS Nano 15 (2021) 19394–19408.
[25] N.N. Zheng, W.Y. Kong, Z. Huang, et al., Rare Met. 41 (2021) 45–55.
[26] S. Xiang, Z. Fan, Z. Ye, et al., Nano Res. 15 (2021) 907–918.
[27] S. Saidin, M.A. Jumat, N.A.A. Mohd Amin, A.S. Saleh Al-Hammadi, Mater. Sci. Eng. C 118 (2021) 111382.

[28] M. Huo, L. Wang, Y. Chen, J. Shi, Nat. Commun. 8 (2017) 357.
[29] G. Guo, H. Zhang, H. Shen, et al., ACS Nano 14 (2020) 13391–13405.
[30] Z. Xu, G. Liu, P. Liu, et al., Acta Biomater. 147 (2022) 147–157.
[31] F. Shao, Y. Wu, Z. Tian, S. Liu, Biomaterials 274 (2021) 120869.
[32] N. Zheng, Y. Fu, X. Liu, et al., J. Mater. Chem. B 10 (2022) 637–645.
[33] Y. Li, L. Wang, H. Liu, et al., Small 17 (2021) 2100756.
[34] Z. Sun, W. Song, G. Zhao, H. Wang, Cellulose 24 (2017) 4383–4392.
[35] S. Mallakpour, M. Madani, Ind. Eng. Chem. Res. 55 (2016) 8349–8356.
[36] X. Liu, Z. Yan, Y. Zhang, et al., ACS Nano 13 (2019) 5222–5230.
[37] Y. Lin, Z. Li, Z. Chen, J. Ren, X. Qu, Biomaterials 34 (2013) 2600–2610.
[38] M. Gong, J. Xiao, H. Li, et al., Mater. Sci. Eng. C 131 (2021) 112522.
[39] S. Fu, R. Yang, J. Ren, et al., ACS Nano 15 (2021) 11953–11969.
[40] S. Guan, X. Liu, Y. Fu, et al., J. Colloid Interface Sci. 608 (2021) 344–354.
[41] X. Wang, C. Li, H. Jin, et al., Chem. Eng. J. 432 (2022) 134438.
[42] X. Cheng, H.D. Xu, H.H. Ran, G. Liang, F.G. Wu, ACS Nano 15 (2021) 8039–8068.
[43] P. Sun, Q. Deng, L. Kang, et al., ACS Nano 14 (2020) 13894–13904.
[44] Z. He, H. Yan, W. Zeng, K. Yang, P. Rong, J. Mater. Chem. B 9 (2021) 1625–1637.
[45] H. Zhao, J. Wang, X. Li, et al., J. Colloid Interface Sci. 604 (2021) 80–90.
[46] T. Xiao, M. He, F. Xu, et al., ACS Nano 15 (2021) 20377–20390.
[47] Z. Wang, B. Liu, Q. Sun, et al., ACS Nano 15 (2021) 12342–12357.
[48] G. Yang, S.Z.F. Phua, A.K. Bindra, Y. Zhao, Adv. Mater. 31 (2019) e1805730.
[49] N. Zheng, Q. Wang, C. Li, et al., Adv. Healthc. Mater. 10 (2021) 2002024.
[50] W. Zhang, C. Yang, Z. Lei, et al., ACS Appl. Mater. Interfaces 11 (2019) 25691–25701.
[51] S. Guan, X. Liu, C. Li, et al., Small 18 (2022) e2107160.
[52] T. Huang, B. Yuan, W. Jiang, et al., J. Mater. Chem. B 9 (2021) 6190–6200.
[53] X. Du, B. Jia, W. Wang, et al., J. Nanobiotechnol. 20 (2022) 12.
[54] M. Shi, Z. Du, Y. Qi, et al., Theranostics 12 (2022) 2658–2673.
[55] A. Moeini, P. Pedram, P. Makvandi, M. Malinconico, G. Gomez d'Ayala, Carbohydr. Polym. 233 (2020) 115839.
[56] C.H. Wang, J.H. Cherng, C.C. Liu, et al., Int. J. Mol. Sci. 22 (2021) 7067.
[57] M. Lu, A. Qu, S. Li, et al., Angew. Chem. Int. Ed. 59 (2020) 8698–8705.
[58] G. Halimu, Q. Zhang, L. Liu, et al., J. Hazard. Mater. 430 (2022) 128485.